PNAS
www.pnas.org

Supplementary Information for

Observation of liquid glass in suspensions of ellipsoidal colloids

Jörg Roller, Aleena Laganapan, Janne-Mieke Meijer, Matthias Fuchs, Andreas Zumbusch

Corresponding Authors Matthias Fuchs, Andreas Zumbusch.
E-mail: matthias.fuchs@uni-konstanz.de,
E-mail: andreas.zumbusch@uni-konstanz.de

This PDF file includes:

Supporting Information Text

Control experiments and fit parameters. As expected for dilute systems, the curves for all determined correlation functions can be superimposed for volume fractions ϕ below the glass transition. This requires that the density correlators $F_s(q,t)$ for several values of q are plotted versus $\log(\Delta t q^2)$ and the orientational correlators $L_n(t)$ are plotted against $\log(\Delta t n^2)$) (Fig. S1).

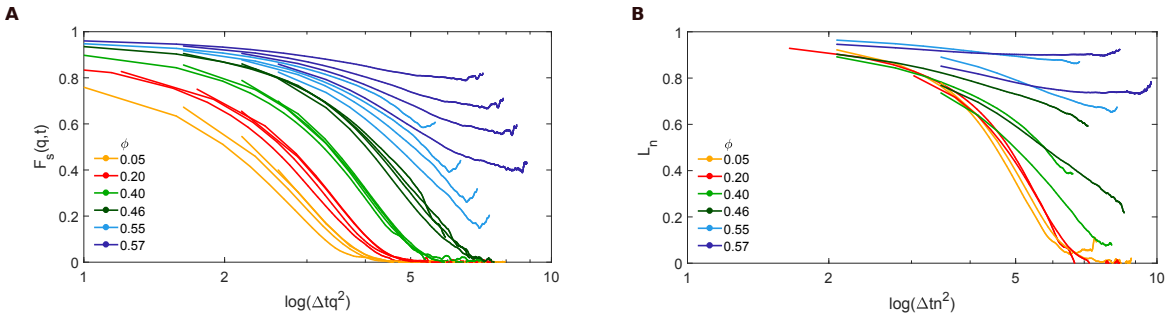

Fig. S1. Superposition of the correlation functions. For packing densities below the glass transition, the values obtained for the density correlator $F_s(q,t)$ at different values of q can be superimposed if they are plotted versus $\log(\Delta t q^2)$ (**A**). The four depicted wavevectors lie in the range $5.18 < q \cdot 2b < 7.90$. Superposition is also possible when the orientational correlators $L_n(t)$ are plotted against $\log(\Delta t n^2)$ (**B**) for $\phi < \phi_c$. Here, correlators for $n = 2$ and 4 are shown.

The data on the systems's dynamics shown in the main text were measured several times for each volume fraction. A combination of all the measured data is shown in Fig. S2A,B, where we plotted the mean squared displacement (MSD) $\langle \Delta r^2 \rangle$ and the mean squared angular displacement (MSAD) $\langle \Delta \theta^2 \rangle$ for all measurements. Since the data nicely collapse onto one curve for each ϕ, for clarity plots containing just single curves are shown in the main text. To evaluate the homogeneity of the particle movements along the axes parallel $\langle \Delta r^2 \rangle_{||}$ and perpendicular $\langle \Delta r^2 \rangle_{\perp}$ to the orientation axis of an ellipsoid, we separately analyzed the respective MSDs (Fig. S2C,D). From fits to the data, we obtained short time diffusion coefficients $D_{||}$ and $D_{\perp}$. As expected, particles tend to move faster along the orientation axis than perpendicular to it as is shown in the plot $D_{||}/D_{\perp}$. While these ratios slightly increase with ϕ and have a maximum in the liquid glass state at $\phi = 0.55$, they hardly deviate from the values expected for a freely diffusing ellipsoidal particle indicated by the dashed line in Fig. S2E *((1))*.

As described in the main text, we fitted the obtained correlation functions to the Kohlrausch-function (Eq. 4). Only curves which showed a clear decay within the measured time window were fitted; representative examples are shown in Fig. 3C,D. Fit parameters are collected in Table 1.

ϕ	0.05	0.2	0.4	0.46	0.55
translation ($q = 3.2\mu m^{-1}$)	0.95774	0.88347	0.81916	0.62496	0.39930
rotation ($n = 4$)	0.77396	0.74768	0.53068	0.33530	

Kohlrausch β parameter for the fits shown in Fig. 3 B and D. The amplitudes f_Φ were set to unity to reduce the number of fit parameters.

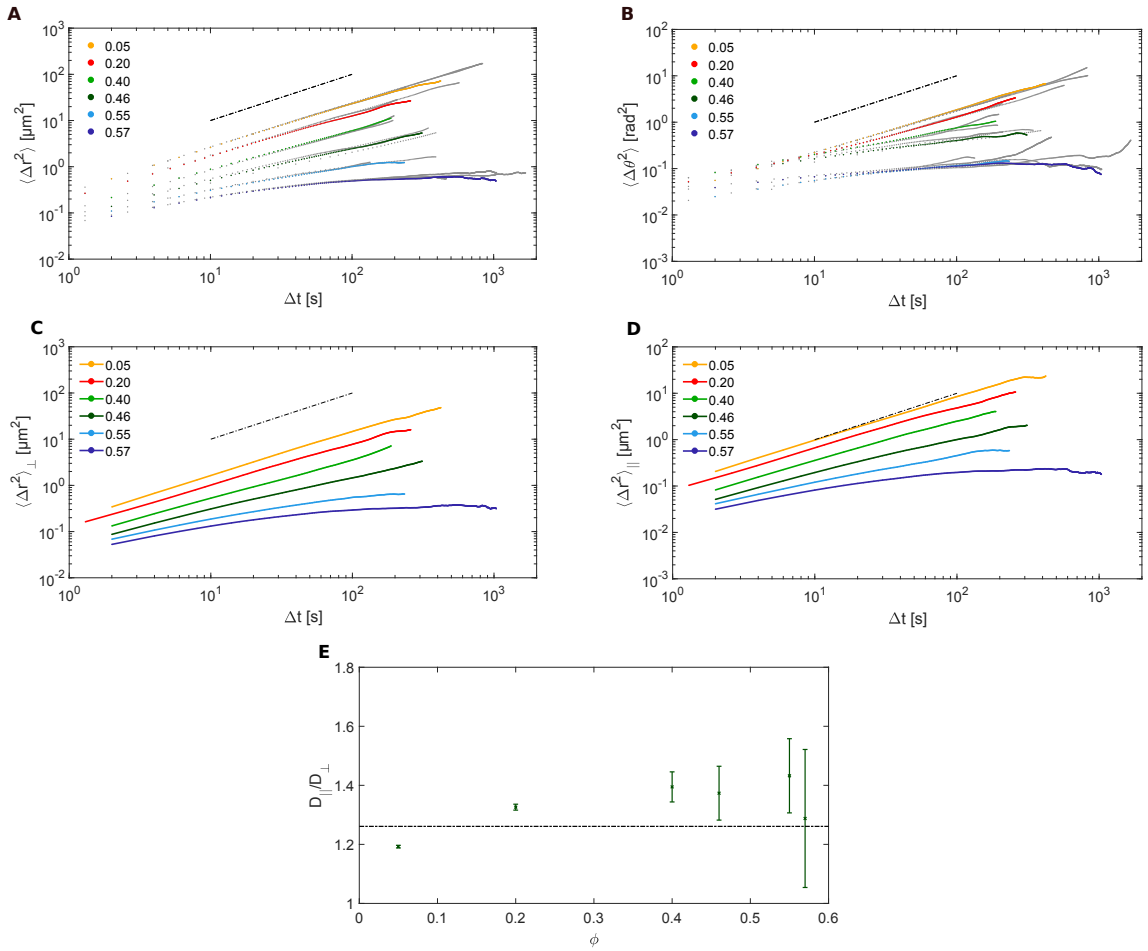

Fig. S2. Experimental data showing the mean squared displacement (MSD) $\langle \mathbf{\Delta r^2} \rangle$ (A) and mean squared angular displacement (MSAD) $\langle \mathbf{\Delta \theta^2} \rangle$ (B) for all measured samples (grey lines). Very good coincidence is found for subsequent measurements at the same ϕ. Therefore only one measurement for each ϕ is shown in the main text which appears to be a good representative (colored lines). The dotted line indicates the slope $m = 1$ which shows the free diffusive behaviour. Additional calculation of the mean squared displacement perpendicular $\langle \Delta r^2 \rangle_\perp$ (**C**) and parallel $\langle \Delta r^2 \rangle_{||}$ (**D**) to the orientation axis of an ellipsoid from the experiments. (**E**) The ratio of the obtained diffusion coefficients, the vertical dashed line illustrates the value for a free particle derived in Ref. (1).

Details on the simulation results. Fig. S3 shows the correlation functions, $F_s(q,t)$, $L_2(t)$, $L_4(t)$ and the order parameter S for the systems with periodic boundary conditions. Similar to De Michele et al. (2), the isotropic-nematic threshold was set to $S = 0.3$, hence the nematic transition is at $\phi \approx 0.49$. For nematic systems, $F_s(q,t)$ monotonically decreases to 0 without significant stretching, while $L_2(t)$ tends to form a plateau that corresponds to the orientational ordering. We verified the formation of a nematic state in these systems by calculating the plateau height of $L_2(t)$ and the final value of S^2 (3),

$$\lim_{t\to\infty} L_2(t) = S^2 \qquad [S1]$$

For the nematic systems obtained in the simulations, the final values of $L_2(t)$ are close to the S^2 values despite the finite time and finite size of the box.

Fig. S4 shows $F_s(q,t)$, $L_2(t)$, $L_4(t)$ and S for the systems with rough walls. In this figure, the characteristic plateau formation for glasses can be observed. Unlike the systems with periodic boundary conditions (Fig. S3), the corresponding $|S|$ values for the systems with rough walls are all below 0.3. Plateaus are clearly observed starting at $\phi = 0.55$. The $L_2(t)$ plateau value is ≈ 0.8 and Eq. (S1) is no longer obeyed. Instead, the plateau values are used for the von Schweidler fits for glassy systems as discussed in the main text.

$S_{lm}(q)$ is an orientation-dependent structure factor that can be used to analyze the correlation of the orientations of the ellipsoids. It is defined as

$$S_{lm}(q) = \frac{1}{N} \langle \rho^*_{lm}(q) \rho_{lm}(q) \rangle, \qquad [S2]$$

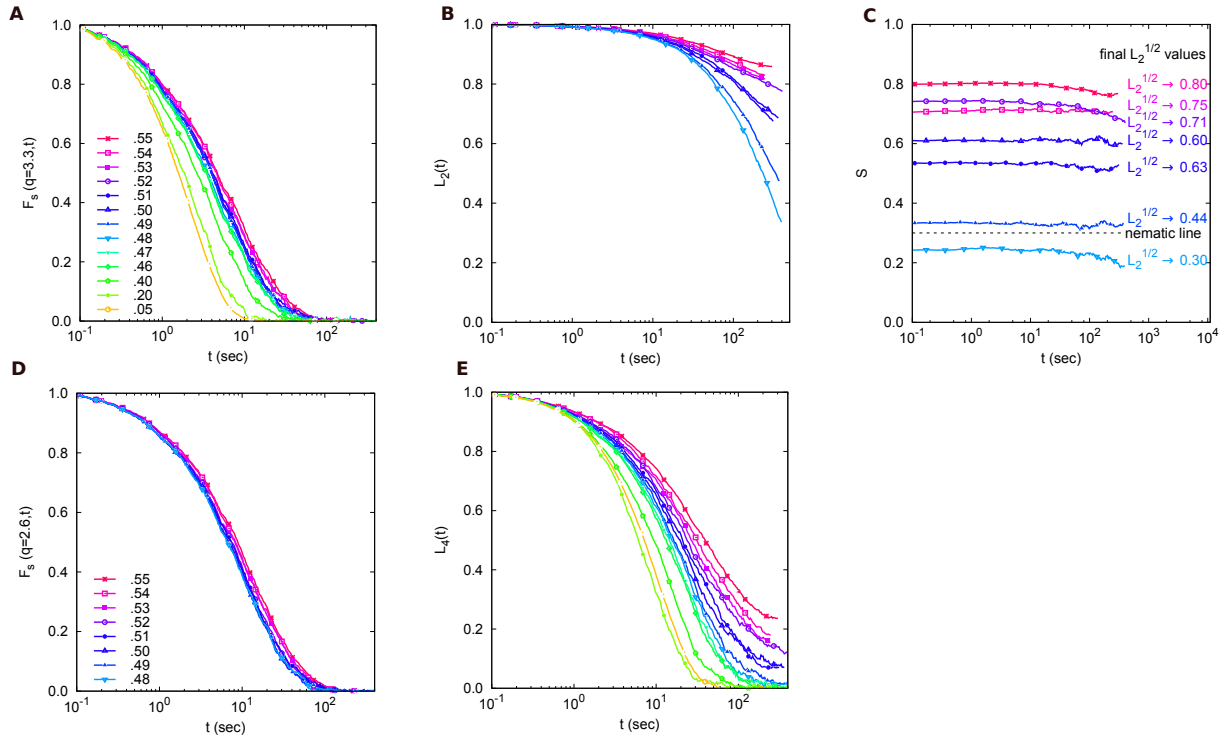

Fig. S3. Data from BD simulations with periodic boundary conditions for $\mathbf{F_s(q,t)}$ (A), $\mathbf{L_2(t)}$ (B) and S (C) where the plateau formation is attributed to nematic ordering starting at $\phi = 0.49$. Figure legend of part **A** also applies to **B,C**. Additional data for $F_s(q,t)$ (**D**) and $L_4(t)$ (**E**)

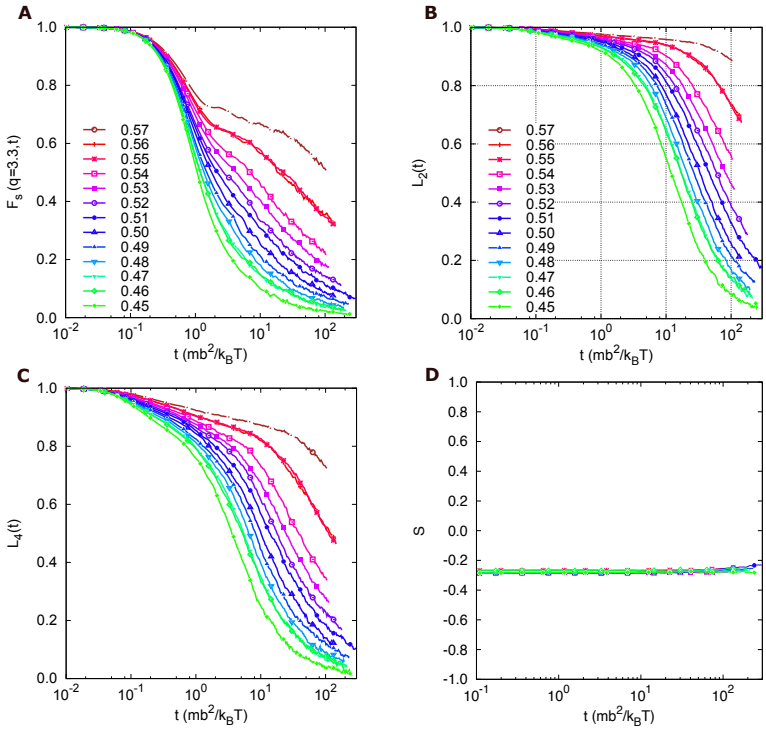

Fig. S4. Data from MD simulations with rough walls for $\mathbf{F_s(q,t)}$ (A), $\mathbf{L_2(t)}$ (B), $\mathbf{L_4(t)}$ (C) and S (D). The plateau formation for high packing fractions is attributed to glass formation at $\phi \approx 0.56$. Figure legend of part **B** also applies to **C** and **D**.

with the microscopic density defined as

$$\rho_{lm}(q) = \sqrt{4\pi} i^l \sum_{j=1}^{N} e^{i\mathbf{q}\cdot\mathbf{r}_j} Y_{lm}(\mathbf{\Omega}_j), \qquad [S3]$$

where $Y_{lm}(\mathbf{\Omega})$ is the spherical harmonic function for Euler angles $\mathbf{\Omega}(\theta, \phi)$. Note that we only consider the diagonal terms of the orientation-dependent structure factor. The results for $l = 2, m = 0$ in the simulations (using periodic boundary conditions) are shown in Fig. S5. The transition to a nematic phase in the simulations is reflected in S_{20} in two ways. First, for small q-vectors, S_{20} increases as ϕ increases, signaling the formation of long-range order that is limited to the size of the simulation box. Second, the neighbor peak of S_{20} starts to become more visible and shifts to the right as ϕ increases. That is, the favored alignment of neighboring ellipsoids is such that their axes of symmetry (a) are parallel to each other.

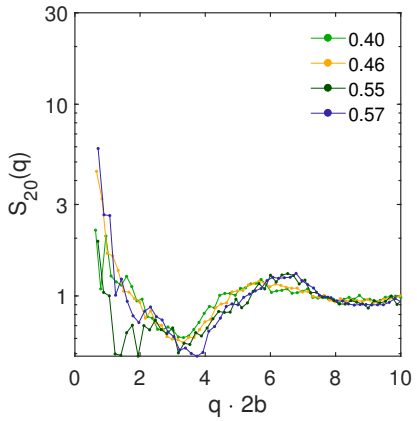

Fig. S5. Simulation counterpart of Fig. 5F of the main text. Calculated $\mathbf{S_{20}(q)}$ shows the nematic transition for $\phi > \mathbf{0.46}$, indicated by the right shift of the first peak.

Mode coupling theory. We argue that the region of liquid glass in phase space is bounded by two glass transitions at fixed aspect ratio, providing the basis for our MCT glass stability analysis in the main text and extending the previous MCT calculations (4); there the possibility of a glass-to-glass transition was not explored.

The transition of a fluid of hard ellipsoids to a liquid glass was found by MCT in a fully microscopic calculation. It was shown to be driven by long-range nematic correlations which arise close to the equilibrium isotropic-nematic transition (see Fig. 5F recording these correlations in the samples). The transition line meets another line of fluid to glass transitions, which extends to the MCT hard sphere transition for aspect ratio approaching unity. It is driven by an increase of liquid short range structure seen in $S(q)$ ('cage effect'; see Fig. 1D). As MCT glass transitions are fold bifurcations in a nonlinear algebraic system, transition lines do not stop when they meet but rather intersect generically. A schematic model shows that the latter transition line extends into the glassy region above the transition to the liquid glass. There it gives a line of liquid glass to glass transitions which is in agreement with the experimental observations.

Starting point is the model by Bosse and Krieger (5) (BK). It describes the generic coupling of two degrees of freedom in the case of a single (discontinuous or generic (6)) glass transition. Their correlators $\Phi_1(t)$ and $\Phi_2(t)$ shall correspond to $L_n(t)$ and $F_s(q, t)$, respectively. The $\Phi_i(t)$ obey Zwanzig-Mori equations with memory kernels $m_i(t)$ (for $i = 1, 2$) given as a general quadratic form. The slowing-down of the correlators' relaxation arises from the feedback in the retarded friction kernels modeled by $m_1(t) = v_1\Phi_1(t)^2 + v_2\Phi_2(t)^2$ and $m_2^{\mathrm{BK}}(t) = v_3\Phi_1(t)\Phi_2(t)$. We generalize the model by including a parameter w modeling the coupling of the second dynamical mode to itself; viz. $m_2(t) = v_3\Phi_1(t)\Phi_2(t) + w\Phi_2(t)^2$. This allows for a second generic glass transition. The two glass transitions of the model will correspond to the B and B' transitions introduced by Letz et al. (4). The parameters v_1 and v_2 encode the increasing orientational friction arising due to slow orientational and translational motion, respectively. Thus v_1 should correlate with the aspect ratio and v_2 with the density. The cross-coupling term v_3 parametrizes the translational friction arising from rotation-translation coupling, while w captures the feedback within the translational motion only. The glass parameters $f_i = \Phi_i(t \to \infty)$ obey the equations $f_i/(1 - f_i) = m_i(t \to \infty)$, where glass transitions appear as bifurcations. Since the model lacks a quadratic coupling of the first mode into the second kernel, it contains a type B' transition at $v_1 = 4$ and v_2 small enough, where f_1 jumps from zero to a finite value, while $\Phi_2(t)$ remains fluid like. For parameter sets with a second transition from fluid to glass, which is continuous in the BK-model ($w = 0$) and discontinuous for $w > 1$, the schematic model shows that this B line cannot terminate at the intersection with the B'-line. Rather, it continues into the glass region, so that there exist two different glass states separated by a line of glass-to-glass transitions. Fig. S6 gives the pertinent states diagram of the model. Choosing an overdamped dynamics with initial time-scale τ_0 in both correlators (see Eq. (4.34), p. 203 of Ref. (6)), typical correlation functions for the fluid (blue), liquid glass (orange), and glass (green) state are depicted in Fig. S6 as well. In liquid glass states, $\Phi_1(t)$ arrests at a finite plateau while $\Phi_2(t)$ decays to zero.

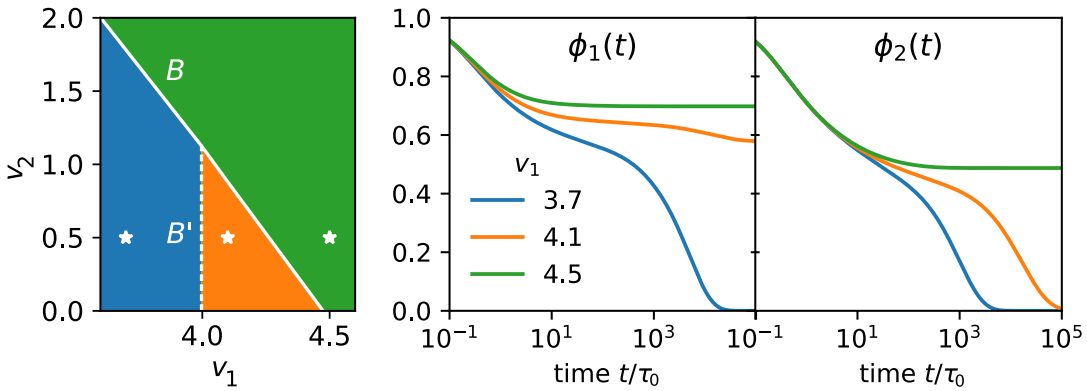

Fig. S6 Schematic MCT model capturing the generic glass transition scenario of two modes: The left panel shows the states diagram at fixed $v_3 = 0.7$ and $w = 3$, where two discontinuous bifurcations exist. They separate fluid ($f_1 = 0$, $f_2 = 0$, blue) from liquid glass ($f_1 > 0$, $f_2 = 0$, orange) and glass ($f_1 > 0$, $f_2 > 0$, green) states. Parameters v_1 and v_2 mimick aspect ratio and density. The other panels show the correlators: The middle panels shows $\Phi_1(t)$ modeling orientational motion (viz. $L_n(t)$), and the right panel $\Phi_2(t)$ modeling translational motion (viz. $F_s(q,t)$); the overdamped MCT equations of motion are solved for the points marked by stars in the states diagram (precise values are $v_1 = 3.7$, 4.1, 4.5 at $v_2 = 0.5$).

References

1. J Happel, H Brenner, *Low Reynolds number hydrodynamics.* (Springer Netherlands), (1983).
2. C De Michele, R Schilling, F Sciortino, Dynamics of uniaxial hard ellipsoids. *Phys. Rev. Lett.* **98**, 265702 (2007).
3. R Eppenga, D.Frenkel, Monte carlo study of the isotropic and nematic phases of infinitely thin hard platelets. *Mol. Phys.* **52**, 1303–1334 (1984).
4. M Letz, R Schilling, A Latz, Ideal glass transitions for hard ellipsoids. *Phys. Rev. E* **62**, 5173–5178 (2000).
5. U Krieger, J Bosse, α relaxation of a simple molten salt near the glass transition. *Phys. Rev. Lett.* **59**, 1601–1604 (1987).
6. W Götze, *Complex Dynamics of Glass-Forming Liquids: A Mode-Coupling Theory.* (Oxford University Press), (2009).